

Corrosion Evaluation of AISI-309 Exposed to 50 mol% Na₂SO₄-50 mol% V₂O₅ at High Temperature Applying Electrochemical Techniques and the Weight Loss Method

Cecilia Cuevas Arteaga

Centro de Investigación en Ingeniería y Ciencia Aplicadas – UAEM, Av. Universidad 1001, Col. Chamilpa C.P. 62209, Cuernavaca, Morelos, México

*E-mail: ccuevas@uaem.mx

Received: 5 October 2012 / Accepted: 23 October 2012 / Published: 1 December 2012

Corrosion performance of stainless steel AISI-309 obtained from electrochemical noise technique and the conventional weight loss method during 5 days of exposure in 50 mol% Na₂SO₄-50 mol% V₂O₅ molten salt at 700°C is reported. Polarization curve is also presented, from which the Tafel slopes, the current density corrosion and corrosion potential were obtained. Electrochemical noise signals were analyzed in the time domain to determine the changes in corrosion activity. A statistical analysis obtaining the resistance noise and the localization index is presented as well as the determination of corrosion rates. Corrosion rates were supported by EDS analysis of corrosion products and scanning electron microscopy analysis of corroded samples. Results from optical microscope examination of the corroded samples showed that AISI-309 suffered intergranular corrosion due to the diffusion of sulfur into the matrix of the alloy through the grain boundaries. A corrosion mechanism of stainless steel AISI-309 is proposed accordingly to the noise pattern and the analysis from SEM results, showing that AISI-309 had a corrosion process of three stages, uniform corrosion, rupture and recovery of the passive film and intergranular corrosion.

Keywords: Stainless steel, electrochemical noise, intergranular corrosion, molten salts

1. INTRODUCTION

Molten salt corrosion at high temperature is presented in boilers, gas turbines and furnaces. These equipments use residual fuel oils, which contains certain amounts of impurities such as vanadium (350-600 ppm), sodium (50-200 ppm), and some percentage of sulfur (2.5-4.5 %), besides small concentrations of nickel, iron, calcium, silicon, aluminum, potassium and magnesium. During combustion produce compounds such as Na₂SO₄ and V₂O₅, and other more complex mixtures formed from these two primary salts, which are formed through chemical reactions between the impurities and

between the impurities and combustion gases such as O₂, SO₂, SO₃, also present in that kind of environments. This type of corrosion is called high temperature corrosion by molten salts or hot corrosion [1], occurring on the heated surfaces of superheaters or reheaters, which are between 600 and 650°C. The high temperature corrosion by molten salts is the accelerated oxidation of the materials, which surface is covered by a thin film of molten salts exposed in a gaseous medium [2], producing thinning of materials, and reducing their useful life. The corrosion phenomenon produces a great amount of investment in maintenance; hence, it is necessary to perform research to determine the resistance of alloys with different compositions, which must consider the presence of chromium, nickel, silicon among others. Control of high temperature molten salts corrosion by materials selection has been partially successful through the use of heat resistant iron and nickel base alloys with high chromium content. A significant research has been conducted on the molten salt corrosion of many types of alloys with these characteristics. In 1980 Harada et al. [3] reported that there was not yet a material resistant to the corrosive effects of molten salts. This statement may still be true, even though many types of materials containing different concentrations of chromium, nickel, aluminum and silicon have been studied to obtain their performance in high temperature environments in presence of molten salts.

A characteristic of molten salts is that behave as electrolytes, therefore, hot corrosion is considered of electrochemical nature, involving electron transfer [4]. If molten salt high temperature corrosion is an electrochemical process, it is possible to study this phenomenon utilizing electrochemical techniques, which are based on oxidation and reduction reactions. Electrochemical techniques have been used during several decades to research, measure, and control the corrosion process in aqueous solutions and molten salts. Over time, they have become more sophisticated, such that, nowadays, it is possible to get more detailed information about corrosion processes. The electrochemical techniques more commonly used have been polarization curves, lineal polarization resistance, electrochemical impedance spectroscopy, and electrochemical noise in current and potential.

With respect to electrochemical noise (EN), normally this technique has been used to determine the type of corrosion through the potential noise, especially localized corrosion; while the current noise has provided data related with the corrosive activity [5-7]. Current noise patterns can also indicate the corrosion mechanism (general or localized) [7,8]. Electrochemical noise technique not only has been used to study aqueous corrosion but also molten salt corrosion [8-10]. EN technique has the advantage to predict the way in which a material is been corroded before seeing the physical attacked surface, which is being exposed in a corrosive medium with no perturbations. Corrosion activity of a material can be followed in time to obtain not only the corrosion rate, but also the type of corrosion, be uniform, localized or mixed corrosion. In addition, some potential and current noise statistical parameters can help to confirm the corrosion performance of metallic materials.

In this paper, the corrosion resistance performance of AISI-309 stainless steel exposed by immersion for 5 days in deep crucible melts of 50 mol% Na₂SO₄-50 mol% V₂O₅ at 700 °C was evaluated. Two electrochemical techniques such as electrochemical noise and polarization curves were used and compared to the weight loss method. Microstructural observations by scanning electron microscopy of the corrosion products of the exposed specimens and the corroded samples freed of

corrosion products, helped to determine qualitatively the internal resistance of the stainless steel and facilitated the understanding of corrosion mechanism under vanadium-sulphate molten salt.

2. EXPERIMENTAL PROCEDURE

Samples were made of a bar of AISI-309 stainless steel, which composition is 0.2C-0.75Si-2.0Mn-23.0Cr-13.5Ni-BalFe. The bar was cut as small rectangular parallelepipeds sized 10x5x2 mm, ground from 120 to 600 grit silicon carbide paper, rinsed with distilled water, degreased with ethyl alcohol and dried under a warm air stream. The specimens as the working electrodes were spot welded to 80% (wt.) Cr-20Ni wire (200 mm long, and 1.0 mm in diameter). This wire was used as electrical connection between the working electrode and the potentiostat. For isolating the 80Cr-20Ni wire from the molten salt, ceramic tubes were used. The gap between the ceramic tube and the electrical connection wire was filled with refractory cement. The 50 mol% Na₂SO₄-50 mol% V₂O₅ mixture was prepared with analytical reagent and was milled for two hours. Known amounts of the solid salts (1500 mg/cm²) of the initial area of the specimen were introduced into a 30 ml silica crucible, to give a melt depth of about 3 cm. Then the silica crucible was set inside an electrical tube furnace to reach the test temperature of 700°C, which was measured constantly during the tests using a type K thermocouple and controlled to ±3°C respect to the test temperature. The crucible together with the solid corrosive salt was replaced for each experiment. It is important to point out that in high temperature corrosion processes, alloys are covered with a thin molten salt layer and with a corrosive gas atmosphere, whereas the experimental procedure carried out in this work were deep melt tests in static air; therefore the experimental conditions and corrosion rates obtained are not representative of fireside corrosion conditions. However, bulk molten salt tests are a viable scheme for material corrosion evaluation. The size and preparation of specimens, as well as the preparation of corrosion mixture were the same for weight loss, potentiodynamic polarization test, and electrochemical noise measurements.

The electrochemical cell for electrochemical noise measurements was a three-electrode setup including two 'identical' working electrodes and 1mm diameter platinum wire as the reference electrode. The platinum electrode was cleaned, abraded on 600-grit SiC paper, washed with ethyl alcohol, and dried. This reference electrode has been used widely, under similar molten salt conditions [10-12]. To obtain stationary conditions, the electrochemical cells were immersed for 40 min before commencing the test. For polarization curves the three-electrode setup included a working electrode and two 1 mm diameter platinum wires as auxiliary (counter) and reference electrode. All platinum wires were isolated in ceramic tubes and sealed with refractory cement, leaving 5 mm long free to contact with the molten salt.

The simultaneous electrochemical current and potential noise were carried out through an ACM Instruments zero-resistance ammeter (ZRA) coupled to a personal computer, which was used to control and store the data for further analysis. The electrochemical noise data were recorded with a sampling frequency of 1 Hz; 1024 measurements were obtained each two hours during 5 days of immersion. Polarization curve was accomplished potentiodynamically polarizing the specimen from -300 mV to + 2000 mV with respect to the corrosion potential at a scan rate of 1 mV/s. The selection of

this scan rate has been previously published elsewhere [13]. The sweep rate of 1 mV/s has been also reported in any other works [3,4,14-17]. Electrochemical polarization curves were made using an ACM Instruments Auto DC potentiostat, also controlled by a personal computer.

Weight-loss measurements were also taken after immersion exposures of 5 days in the same molten salt and temperature conditions. The procedure was made according to ASTM Standards G1 and G31 [18,19] using specimens (triplicate) of the same size as for the electrochemical noise tests. The samples were weighed before and after exposure by means of an analytical digital balance with a precision of 0.0001 g. Three specimens were totally packed in the corrosive mixture contained in independent silica crucibles, and then they were introduced in an electric furnace in a static air atmosphere. The corrosion products were removed from two corroded alloys by mechanical, ultrasonic and chemical cleaning according to ASTM G1. The mass loss was obtained from the two cleaned samples. The third sample was kept to be analyzed by SEM.

The mechanical procedure consisted in cleaning the surfaces of specimens in a repetitively way until the surfaces were free of corrosion products, being the mass loss determined after each cleaning by weighing the specimens. The specimens were scrapped with a sharp metallic tool, trying to get out the solid scales. From time to time, the specimens were observed by means of an optical microscope, which was useful to determine the remains of corrosion products. In this way, the probability to affect the real weight loss measurement was tried to keep it low. The evaluation of the corrosion rate was determined as weight loss by means of calculating the difference between the initial and final weight divided by the initial area of specimens. The third sample from the weight loss method and the specimens as working electrodes from the electrochemical noise technique were mounted (without descaling) in bakelite, metallographically polished and the cross section analyzed by scanning electron microscopy to investigate the morphology and distribution of reaction products. X-ray mapping and microprobe analysis were carried out using a Microspec WDX-3PC system connected to a Zeiss DSM960 scanning electron microscope. In order to determine the type of corrosion attack suffered by the AISI-309, the completely cleaned corroded samples from weigh loss method were also observed through SEM.

3. RESULTS AND DISCUSSION

3.1. Physical Corrosion Characterization

Figure 1 shows 4 micrographs at different magnifications of AISI-309 exposed to 50 mol% Na₂SO₄-V₂O₅ mixture for 5 days at 700°C obtained after using the weight loss method. The images evidence an intergranular corrosion process over the entire surface, clearly showing the grain boundaries. The shape of the grains is irregular, and their sizes lie between 20 µm to 120 µm. Corrosion products are present in the grain boundaries, but also there are hollows in some of these zones. In some regions, corrosion products can be seen outside the grain boundaries covering part of the core of grains. Also, several twins are seen in some grains together with a great amount of pores. The porosity indicates the selective dissolution of some alloying element of the material.

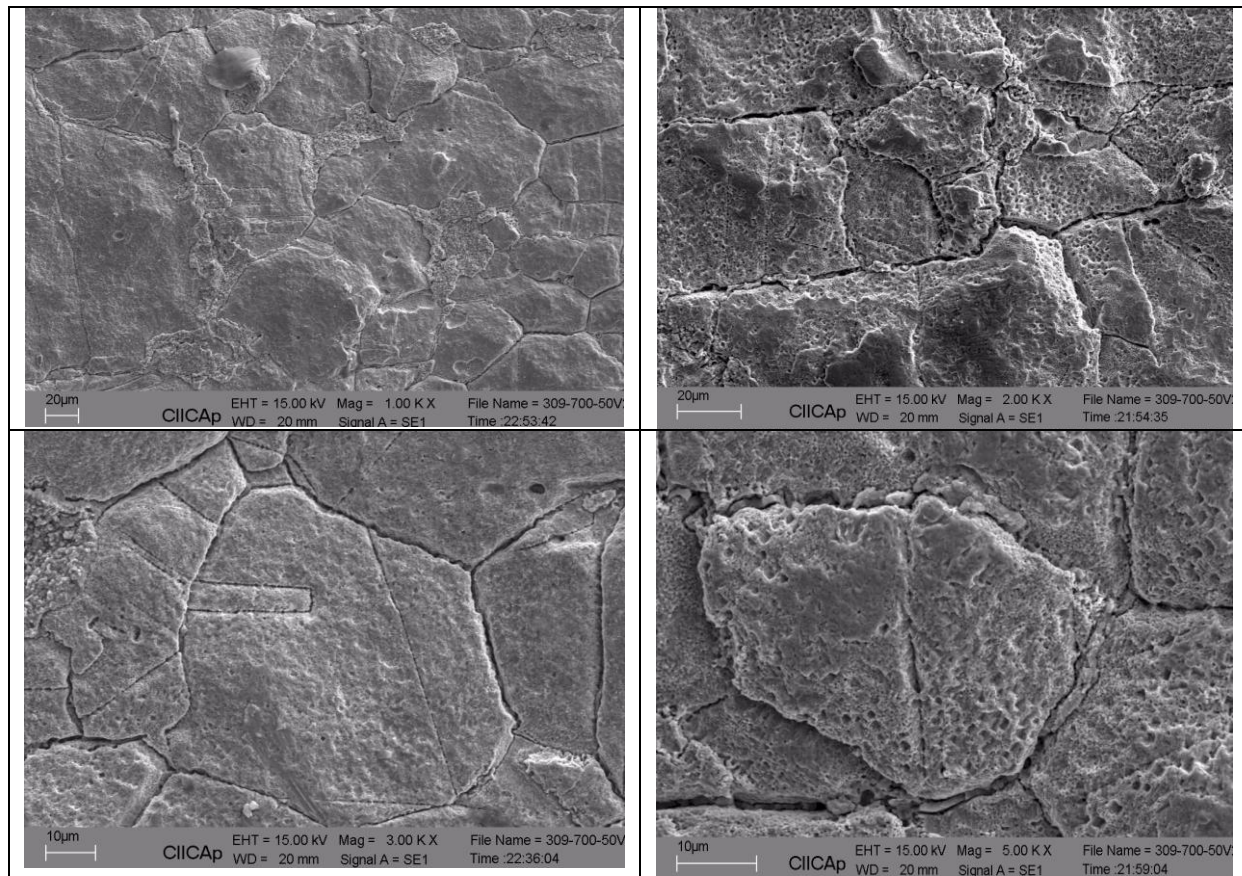


Figure 1. Micrographs of AISI-309 exposed to 50 mol% Na_2SO_4 –50 mol% V_2O_5 mixture for 5 days at 700°C from the weight loss method.

The third sample from the weight loss method was mounted (without de-scaling) in bakelite and metallographically polished. Then it was analyzed in its cross section by scanning electron microscope. Results are presented in Figure 2. The image of Figure 2 shows the interface metal-scale, which has been marked with numbers from 1 to 3. Zone 1 corresponds to the thickness of the AISI-309 which was attacked in an intergranular way. In zone 2, corrosion products just over the surface are expected, whereas zone 3, which is far away from the interface, must contains the corrosion products including the species of the corrosive mixture. In order to determine the composition of the different zones signaled in Figure 2, and determine the type of intergranular corrosion processes, EDS analyzes were made throughout the three zones, which results are presented in Figure 3. The quantitative results of the EDS analyzes are reported in Table 1. The intergranular corrosion process presented in Figure 1 is in accordance with the image presented in Figure 2, since the horizontal strip along the point 1 shows the revealed grain boundaries, which evidence the diffusion of one of the corrosive species inside the material. This diffusion must have been due to the presence of spaces free of one or more alloying elements, which have been oxidized. The penetration of that species was up to 11 μm , although the zone of major intergranular corrosion was of 7 μm of width. Above the intergranular attack, over the metallic surface, it appears a scale with morphology more or less uniform with a thickness around 15 μm .

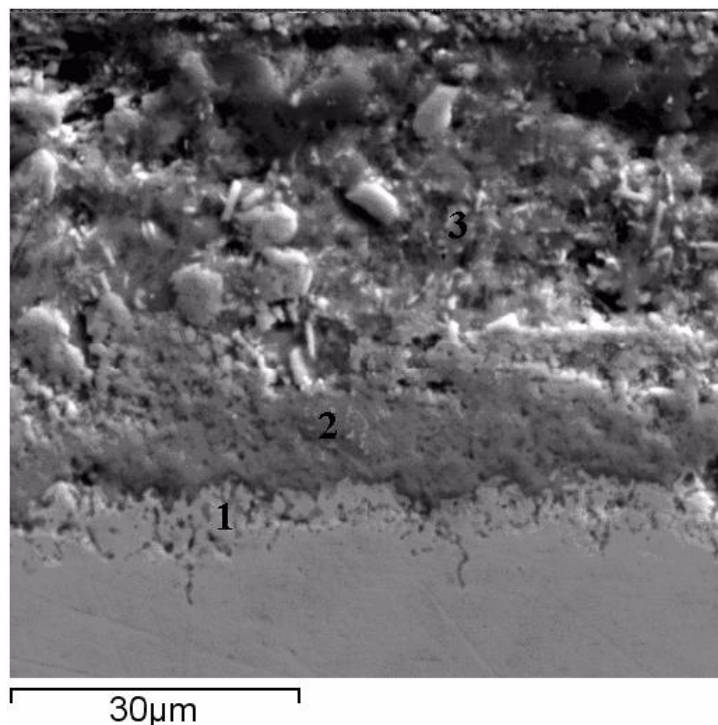


Figure 2. Micrograph of the cross section of the metal-scale interface of the corroded stainless steel AISI-309 exposed to 50 mol% Na₂SO₄-50 mol% V₂O₅ mixture for 5 days at 700°C from the weight loss method.

This scale shows a great amount of pores, through which the corrosive species could diffuse inside the metal. After this scale, there is a thick heterogeneous film, surely composed by porous metallic oxides, species from the corrosive mixture, and secondary compounds formed from the corrosive species and the initially formed metallic oxides. According to the EDS analysis, the intergranular zone is mainly composed of the alloying elements of major composition (Fe, Ni and Cr) and sulfur. The composition of silicon is practically the original one, and the composition of manganese is 0.77 smaller than its original composition, which means that silicon has no participation in the corrosion mechanism suffered by AISI-309, whereas manganese apparently suffered certain oxidation. Taking into account the original composition of the AISI-309, it is possible to observe that the composition of chromium and iron is less than the original one, whereas the composition of nickel was increased in this zone of the alloy.

Table 1. Quantitative results of EDX analysis of the different zones marked in Figure 2.

Espectrum	O	Na	Si	S	V	Cr	Mn	Fe	Ni
Zone 1	0.225	0.000	0.738	3.744	0.014	12.895	1.232	46.854	34.288
Zone 2	35.662	0.000	0.361	3.586	0.086	25.711	0.905	26.231	7.438
Zone 3	26.861	4.306	0.055	1.023	13.56	16.710	0.190	27.667	9.627

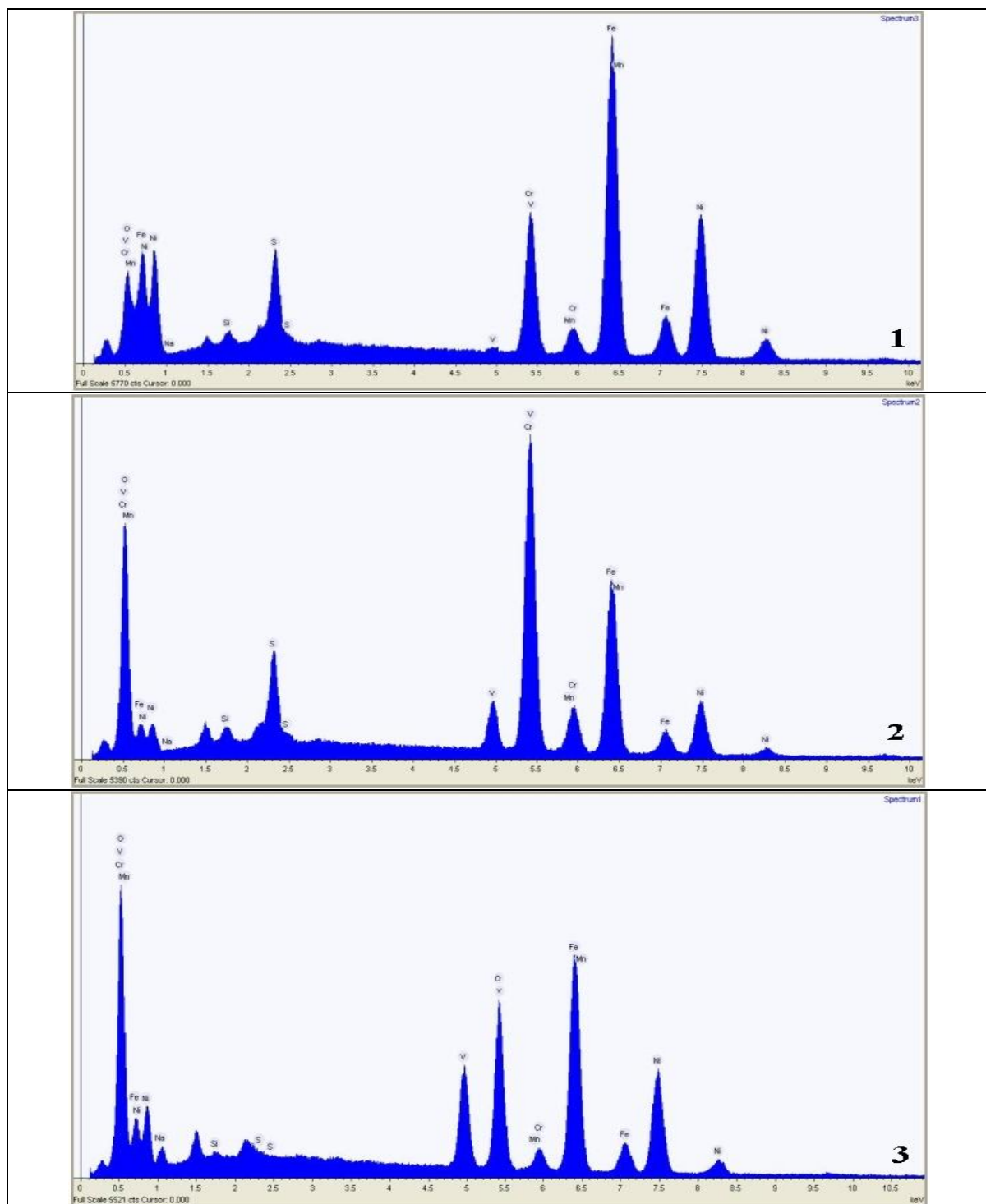


Figure 3. Spectrums of EDS analyzes made to the points marked in Figure 2.

The decreased composition of Fe and Cr must be due to the selective oxidation of these elements. It is possible that the place initially occupied by the chromium and iron inside the alloy has been replaced by the nickel, which has probably diffused from the matrix to the outermost part of the alloy, or maybe the Cr and Fe mass loss produced the Ni enrichment in zone 1. Zone 2 contains a great amount of oxygen, which is chemically combined with chromium, iron and nickel. Sulfur and

vanadium are also present, sulfur almost in the same composition than that in zone 1. The presence of sulfur and vanadium together with oxygen may result in vanadates species [20-22]. Also, the presence of S and V is an evidence of the diffusion of these species from the corrosive mixture throughout the corrosion products formed by metallic oxides. From EDS analysis, it is also confirmed the formation of a great amount of chromium oxide, iron oxide and nickel oxide, being chromium oxide the major component of this zone.

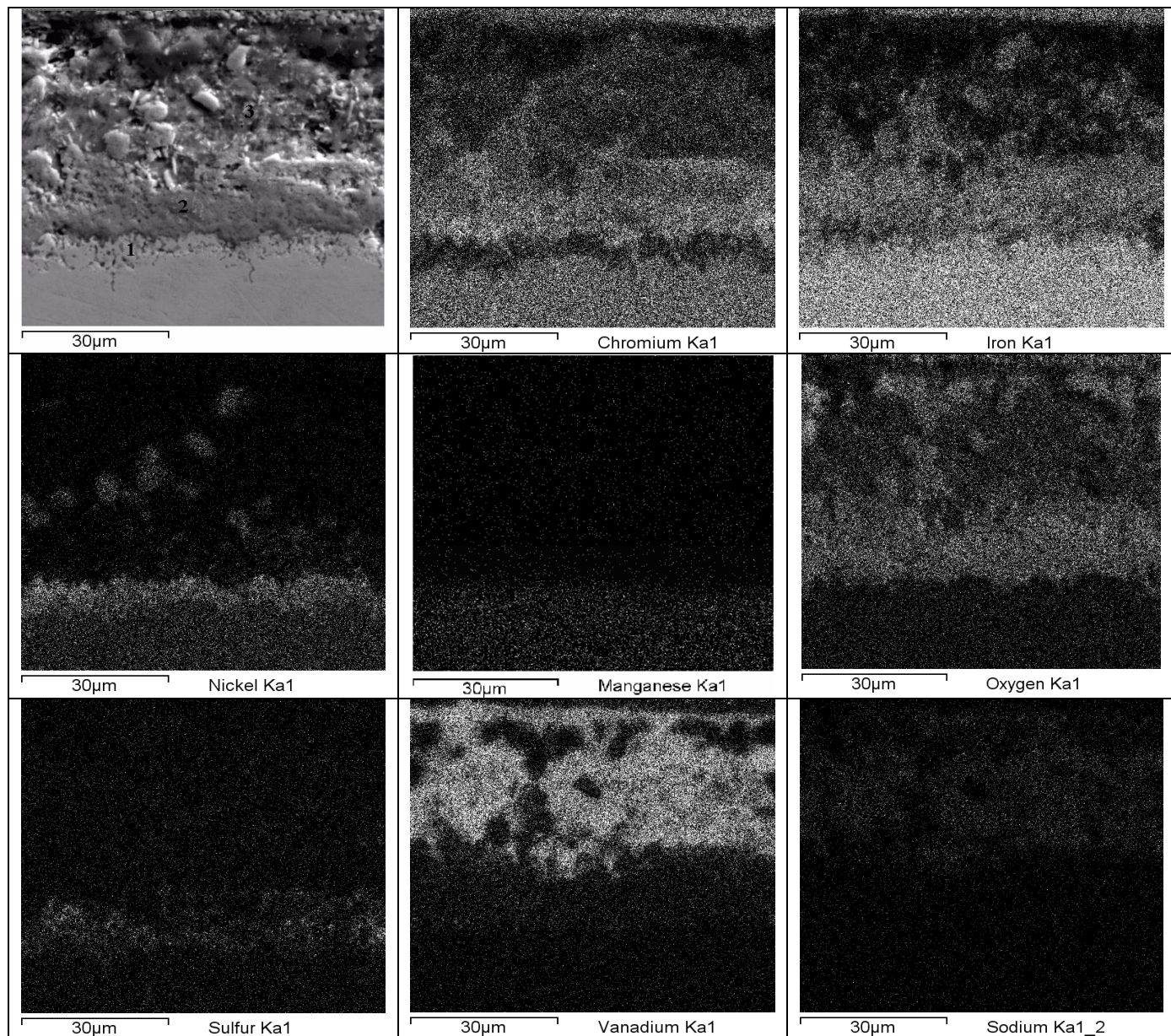


Figure 4. Electron image of the metal–scale interface and X-ray mappings of Cr, Fe, Ni, Mn, O, S, V and Na of AISI-309 exposing 5 days to 50 mol% Na_2SO_4 –50 mol% V_2O_5 at 700 °C.

Silicon and manganese oxides are also presented in a much smaller proportion. The EDS results of zone 3 show the presence of the main species of the corrosive mixture (O, Na, S, and V),

observing that the amount of sulfur was reduced comparatively to that in zone 2, whereas vanadium was incremented, which is due to the major diffusion presented by sulfur inward the metal, which is present above and below the interface metal-scale. Vanadium is only present in the scale just above the mentioned interface. The amount of chromium, silicon and manganese was reduced in this zone, whereas the amount of iron and nickel was incremented with respect to zone 2. The diffusion outward of metallic oxides and their dissolution is evident; hence, there is a film of what it seems to be porous oxides. Figure 4 shows a cross section of the metal–scale interface of the corroded AISI-309 specimen of the same micrograph presented in Figure 2, which as it has been said, was exposed during 5 days to 50 mol% Na₂SO₄–50 mol% V₂O₅ at 700 °C.

X-ray mappings of the main elements constituting the stainless steel alloy together with mappings of oxygen, sulfur, vanadium and sodium. According to the chromium mapping, at the metal surface there is a concentrated 15 µm rich chromium layer, above this, a porous and homogenously dispersed layer of lower chromium concentration is seen, as an evidence of a kind of dissolution suffered by this element due to the chemical interaction with corrosive species. Underneath the concentrated chromium layer, there is a chromium depleted zone of the alloy, which is replaced by a very well defined 6µm thickness film of nickel compound, which is just in the intergranular sulfidation zone inside but in the edges of the substrate. Supported by EDS spectrums of Figure 3 and mappings presented in Figure 4, it can be inferred that at the beginning of the corrosion phenomenon there was a Cr mass loss by the effect of oxidation; afterward such chromium was transformed in a passive layer of Cr₂O₃ as a reaction of the alloy to be protected, then this initially dense and coherent passive layer of chromium oxide was evenly dispersed with a dissolution process as a result of 5 days of immersion. It is possible that the place initially occupied by the chromium inside the alloy has been replaced by the nickel, which has probably diffused from the deeper zones of the matrix of the alloy to the edges enhancing the sulfidation zone of nickel, or maybe the Cr mass loss to form the corrosion layer of Cr₂O₃ produced the Ni enrichment in the alloy edges. The chromium oxide is one of the most protective compounds when molten salts of sodium sulphate and vanadium pentoxide are present [18,23]. With respect to the iron mapping, a little more concentrated layer mixed with the chromium layer is seen. Above this concentrated iron layer, there is a porous and heterogeneous iron layer, with some localized spots more concentrated than that observed for chromium. Certain depletion of iron is also seen just in the interface metal-scale. With respect to the mapping of manganese, it seems not to have had participation during 5 days of exposition. It can be said that dissolution of iron and chromium oxides and in much less extend nickel oxide was carried out. This dissolution has become the presumably protective chromium layer initially formed, in a discontinuous and non coherent oxide layer, which has permitted after 5 days of exposition, the diffusion of sulfur below the metallic surface, causing the internal sulfidation. The oxygen mapping shows a congruent behavior with respect to the iron and chromium mappings in the sense of the existence of iron and chromium oxides in the regions mentioned before. The concentration of sulfur in the interface metal-scales, and in the sulfidation zone is evident, having the confirmation of internal degradation at this time. The chemical interaction between the main elements of the alloy with sulfur in the formation of metallic sulphides must be possible. The internal strip of sulfur coincides with the concentrated nickel film and iron, therefore nickel and iron sulphides may be present. Mapping of vanadium shows that vanadium presents above

the high concentrated chromium and iron layers, just where the porous and heterogeneous chromium and iron layers are localized. The black spots are related with the presence of oxygen, which is associated partially with iron. Accordingly with the mapping of sodium, which is scarcely perceptible, it can be observed that it is linked with vanadium. The clearly layer where vanadium, sodium, oxygen, iron and chromium appear, may result in secondary species in form of iron and chromium vanadates or vanadyl vanadates [24-25]. It is important to note that vanadium did not cross the oxide barrier formed by chromium and iron oxides, which avoid the diffusion of this corrosive species to the metal-scale interface. Nevertheless, the diffusion and introduction of sulfur inside the matrix of AISI-309 was possible, inducing the internal sulfidation.

3.2. Electrochemical Measurements

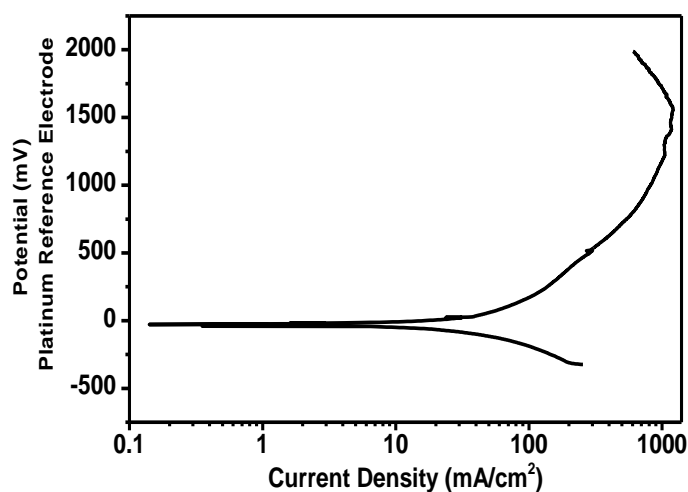


Figure 5. Potentiodynamic Polarization curve of AISI-309 exposed in 50 mol% Na_2SO_4 –50 mol% V_2O_5 at 700 °C.

Figure 5 shows the potentiodynamic polarization curve for AISI-309 stainless steel exposed to 50 mol% Na_2SO_4 –50 mol% V_2O_5 at 700°C. The graph was taken once E_{corr} was stable, which was approximately after 40 min. This curve showed a corrosion potential of -28 mV. Applying the Tafel extrapolation method, the corrosion current density was obtained as 25.54 mA/cm^2 . The Tafel slopes determined by the same method were $b_a = 293.5 \cdot 10 \text{ mV/decade}$ and $b_c = 257.72 \text{ mV/decade}$. For the present study, the polarization curve is important because the anodic and cathodic slopes b_a and b_c were determined to be used in the calculation of corrosion rates from the electrochemical noise through the resistance noise R_n , using the Stearn–Geary equation. The Tafel regions in the polarization curve are not well defined, probably reflecting the importance of mass-transfer conditions, indicating that the diffusion of the species can have a significant influence on the rate controlling step. Tafel slopes lower than 100 mV/dec are typical for activation controlled systems, whereas Tafel slopes with larger values are typical for systems which are not purely activation or diffusion controlled [26]. The polarization

curve shows an active process from the corrosion potential to 1220 mV. Afterwards, a constant current is presented from 1120 mV to 1600mV. A passivation is seen at the end of the curve until 2000mV.

3.3. Electrochemical Noise Technique

Figure 5 shows the most significative series times in current and potential obtained during the exposure time of 5 days of AISI-309 to 50 mol% Na_2SO_4 -50 mol% V_2O_5 at 700 °C. These time series were selected because represent the behavior pattern of AISI-309 along its exposure in the mentioned molten salt. The electrochemical noise time series were used to analyze the changes in corrosion activity for the system under study along the exposure time in molten salts. Figure 5 (a, b, c, d, e, f) shows some selected current and potential time series from the beginning of exposure to 5 days. Even though 120 time series were obtained during the immersion time, just that which represented the general behavior of the corrosion activity were selected. From the mentioned figures, it is observed that apparently AISI-309 suffered three different corrosion stages, the first one from the beginning to 48 hours, the second one after 48 until 92 hours, and the last one after 91 hours until the end of the exposure time. The current and potential time series at 2, 12, 30 and 48 hours of exposure show low amplitude high frequency stochastic oscillations. The current density was decreasing in time, while the potential was increasing. These features agree with the formation of a passivated film, in which the material is protecting it self and potential become nobler. This behavior is in agreement with SEM observations and the results of polarization curve, where it was observed that AISI-309 decreased the current density at the larger potential. Changes in potential are not perceptible in Figure 5.b, nevertheless, Figure 6 shows in detail the time series at 12 and 48 hours, observing in a better way the stochastic oscillations with some small negative and positive transients.

During the second corrosion stage many high-medium transients are observed accompanied with random oscillations. The larger intensity of the transients was 0.007 mA/cm², which is evidence for the nucleation of localized sites or the rupture and recovery of the passive film. It is noticed that current density was decreasing in time, being one order of magnitude smaller with respect to the current density of the time series presented during the first 48 hours.

The values of current density are all positive, which means that one of the two identical electrodes performed preferably as the anode [27,28]. With respect to the potential time series, even though in Fig. 5.d it is not possible to observe clearly the changes in potential, in Figure 6.b, negative transients in potential are observed for 80, 86 and 92 hours. These negative transients correspond to the positive transients in current density, having a correspondence in both noise signals. These results indicate that current and potential signals show a localized behavior of AISI-309 during this stage. The difference between noise signals for a uniform corrosion process and a localized corrosion is evident in Figures 5.a, 5.c and 5.e.

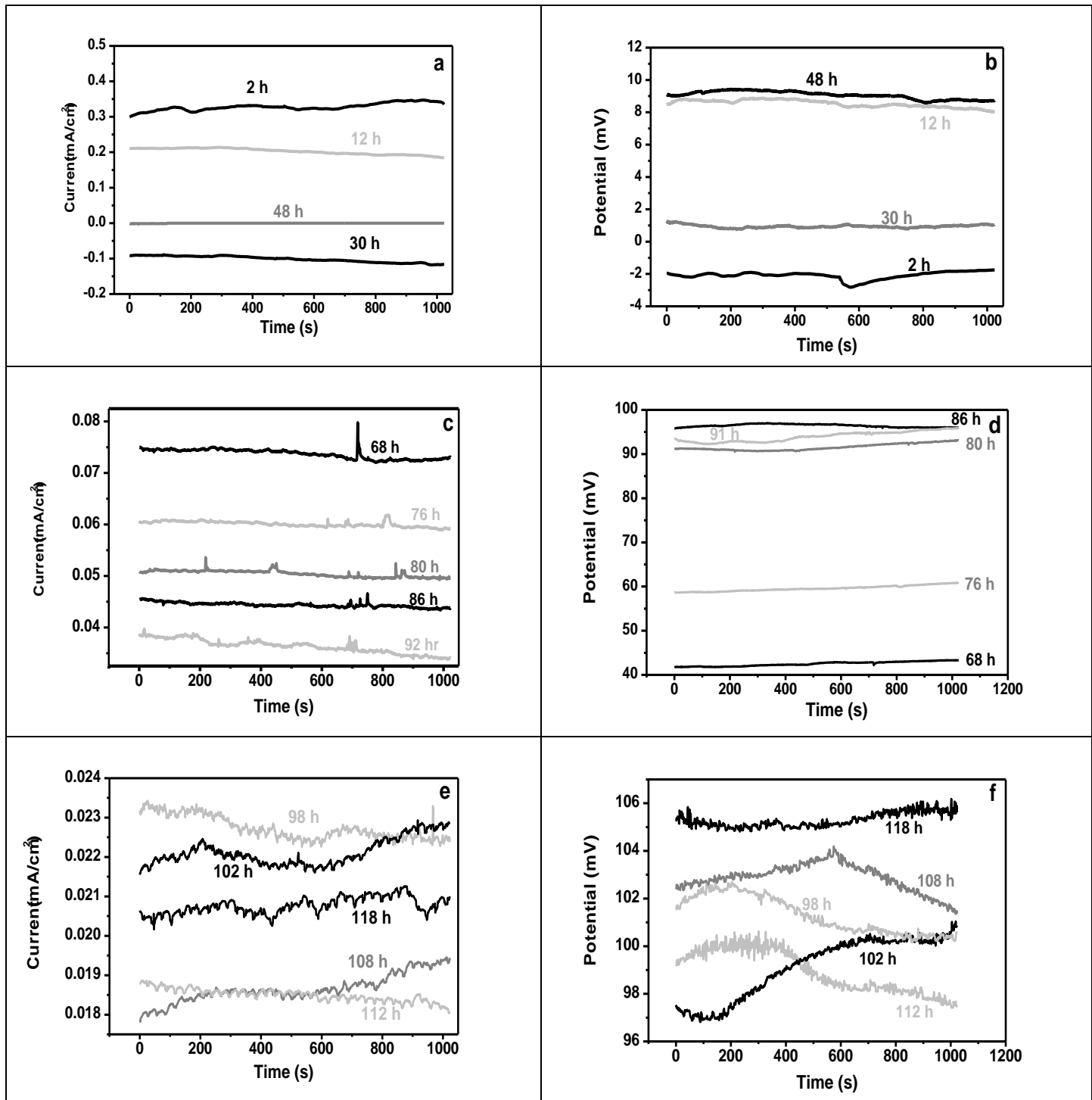


Figure 5. Electrochemical noise in current and potential at different times of AISI-309 exposing 5 days to 50 mol% Na_2SO_4 -50 mol% V_2O_5 at 700 °C.

Third stage, which was practically observed during the fifth day, shows the continuous presence of negative and positive transients practically of the same magnitude and at the same frequency. Those changes in current, where an instantaneous and sudden increment is followed with a current decrement show the presence of a kind of localized events. The potential behavior corresponds very well with the current density signals, in the sense that an increase in current corresponds to a

decrease in potential. After the interpretation of the noise signals, it can be stated that during the first stage, AISI-309 formed a protective film, accordingly with SEM and EDS results, the film could be composed by Cr_2O_3 , NiO and Fe_2O_3 . The corrosion activity seems to have been of low magnitude. During the second stage, which comprised the third and fourth days, the passivated film suffered a broken or localized dissolution, which produced sudden current increments with its corresponding recovery. A kind of localized corrosion is expected. The noise signals of the third stage presented during the fifth day indicates a development of a continuous and specific type of localized corrosion process in a generalized way (through the whole surface). Accordingly with the images presented in Figure 1, the localized corrosion, which is represented by the feature of current and potential time series of figure 5.e and 5.f is intergranular corrosion where sulfur is present accordingly with Figure 2 and the map of sulfur of Figure 4. This kind of localized corrosion is characterized by the formation and dissolution of some chemical species in the grain boundaries. As it has been said above, maps of nickel, iron and sulfur in Figure 4, shows that it is possible the chemical interaction of these species inside the material, indicating the presence of nickel and iron sulphides in the grain boundaries. It can be stated that once the formation of nickel and iron sulphides was carried out, these compounds were partially dissolved, resulting in the morphology presented in Figure 1. The images of Figure 1, especially that with magnification of 3 KX and 5 KX show that it is possible that grains had been dropped, since, the grooves around the grains seem to be very deep. At 5 days of exposure, grain dropping did not happen yet, nevertheless, in such situation, the lost mass could have been very large.

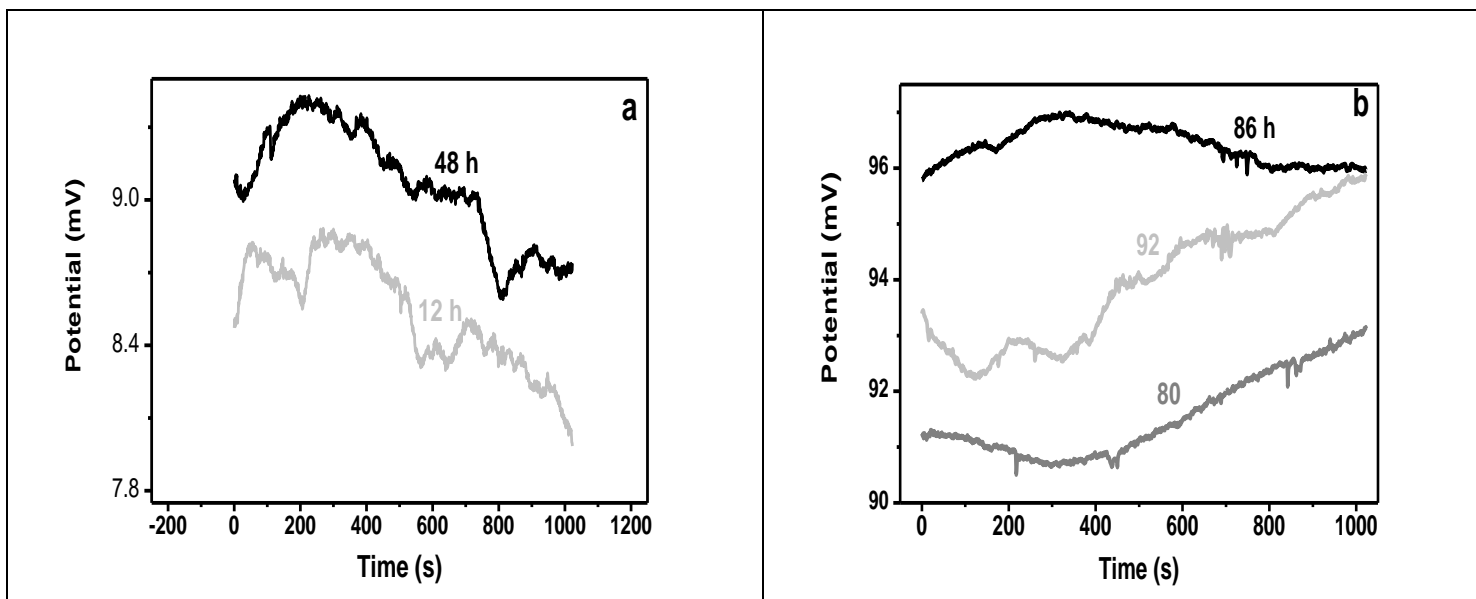


Figure 6. Details of noise potential at different times of AISI-309 exposing 5 days to 50 mol% Na_2SO_4 –50 mol% V_2O_5 at 700 °C.

Fig. 7 presents the localization index of AISI-309 obtained from the noise data. Localization index LI, in some cases can be considered as an indicator of the prevailing corrosion mechanism [29]. This parameter was calculated as the ratio between the current noise standard deviation σ_i , over the root-mean-squared current value I_{rms} [30], the corresponding mathematical relationship has been

reported elsewhere [20,31]. $LI = 0$ is observed for systems for which the individual data points xi show only small deviations from the mean value of current, while $LI = 1$ is observed for $xi \gg$ than the mean value of current. For uniform corrosion, LI values lie between 0.0 and 0.01; for mixed corrosion, between 0.01 and 0.1; and for localized corrosion between 0.1 and 1.0 [30]. From the beginning to one and a half day LI values are the smallest, being most of them in the zone of uniform corrosion, maybe because during this stage the material developed a passivated film. Afterward, LI values incremented, and some of them lie in the zone of localized corrosion, this happened because passivated film suffered nucleation of localized events. Then, LI values lie in the zone of mixed corrosion, which means that both uniform and localized corrosion processes were presented. Accordingly with the physical observations of corroded samples (Figure 1), localized process was performed in grain boundaries, whereas the uniform process over the grain surface, even though, grains surfaces presented a significant porosity. The application of this statistic parameter to current noise signals obtained by the electrochemical noise technique, in this case of study was reliable, being LI an indicator of localized corrosion processes.

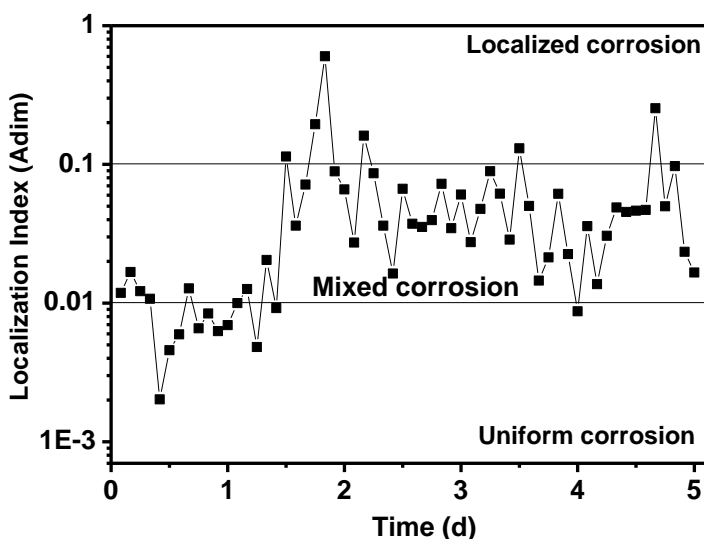


Figure 7. Localization index of the corrosion process for AISI-309 exposed to 50 mol% Na_2SO_4 –50 mol% V_2O_5 at 700 °C.

3.4. Noise Resistance R_n and Mass Loss

Figure 7 shows the experimental mass loss in time obtained from electrochemical noise technique for AISI-309 stainless steel exposed to 50 mol% Na_2SO_4 –50 mol% V_2O_5 at 700 °C. To determine the mass loss in time, the noise resistance R_n (evaluated as the ratio of the potential noise standard deviation over the current noise standard deviation) has been calculated [32-34]. Sixty R_n data during 5 days were obtained. The R_n (ohms.cm^2) data were used in the Stern-Geary equation to obtain I_{corr} (mA/cm^2), and through the use of Faraday's Law [13,35,36], the mass loss was calculated. The Tafel slopes determined from the polarization curve for the test temperature conditions were

determined using the analysis software provided with the potentiostat and used in the Stern-Geary equation [37].

The Stern-Geary equation and Faraday Law are shown in equations 1-4.

$$I_{corr} = \frac{B}{Rn} \quad \text{Eq. [1]}$$

Being B a relationship between the Tafel slopes:

$$B = \frac{b_a b_c}{2.303(b_a + b_c)} \quad \text{Eq. [2]}$$

Applying the Faraday Law, where the mass loss M is given in mg/cm² min:

$$M = K I_{corr} (EW) \quad \text{Eq. [3]}$$

EW is the equivalent weight given by:

$$EW = \frac{1}{\sum \frac{n_i f_i}{AW_i}} \quad \text{Eq. [4]}$$

Where n_i is the number of transferred electrons during oxidation process for each element i of the alloy (2 for Ni, and 3 for Fe and Cr, according to the most stable compounds), f_i is the weight fraction of element i and AW_i is the molecular weight of element i . The mass loss calculated from electrochemical measurements has been compared to the measured weight loss for 5 days of exposure, which results are discussed forward. Figure 8 presents the corrosion kinetics of AISI-309 exposed 5 days to 50 mol% Na₂SO₄-50 mol% V₂O₅ at 700°C obtained from the electrochemical noise techniques accordingly to the equations 1-4. Figure 8.a shows the instantaneous (each 2 hours) corrosion rate, which begins with low values during the first hours (less than 0.1 mg/cm²), and then behaves in oscillatory way between a range of 0.1 to 1.0 mg/cm² until the fourth day. After that, corrosion rate increases until one order of magnitude. This behavior corresponds to the corrosion activity presented by the electrochemical noise signals, observing that at the beginning of corrosion process a passive film was formed, and then the oscillations of corrosion rate indicate the rupture and recovery of the passive film during the formation of localized corrosion events. At the end of the exposure time, the increase in corrosion rate is expected due to the presence of intergranular attack by means of the species sulfur, which has been stated in the physical characterization of corroded samples (Figures 1, 2 and 4).

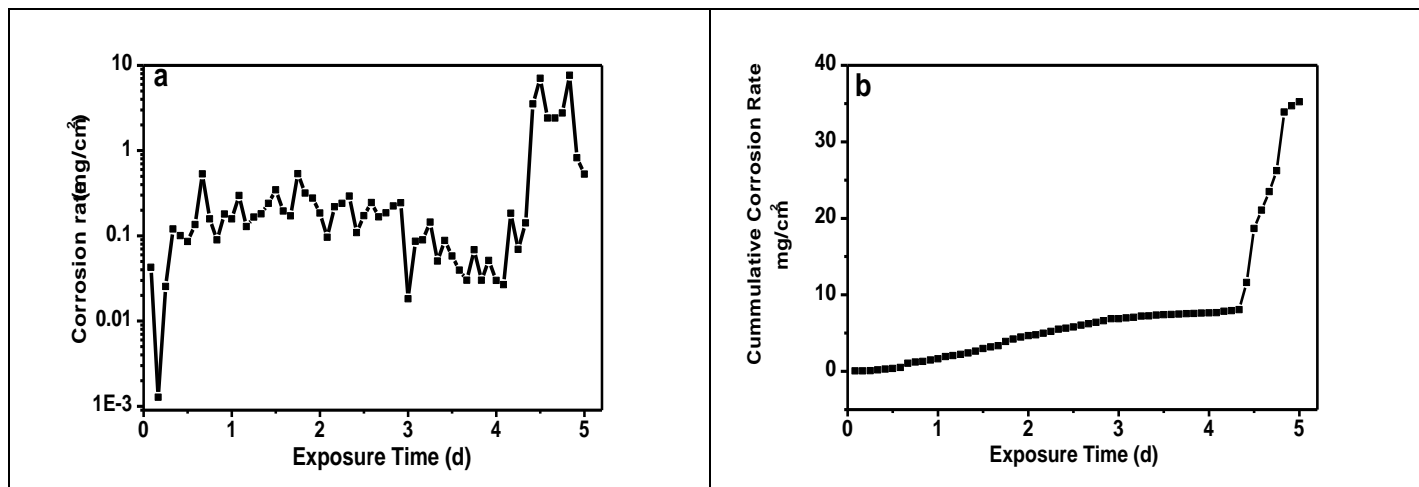


Figure 8. Corrosion kinetics of AISI-309 exposed 5 days to 50 mol% Na_2SO_4 –50 mol% V_2O_5 at 700°C, (a) instantaneous corrosion rate, (b) cumulative corrosion rate.

The increase in corrosion rate is also due to the selective oxidation over the metallic surface, since, a great porosity was observed. Figure 8.b presents the cumulative corrosion rate of AISI-309, observing that during the four firsts days corrosion rate increment with a much smaller trend with respect to that at the last day of exposure time. The weight loss obtained from the conventional weight loss method after 5 days of exposure was $27.38 \text{ mg}/\text{cm}^2$, whereas that obtained from the electrochemical noise through R_n was $35.38 \text{ mg}/\text{cm}^2$. These results present a very small difference, which may be due to excessive cleaning made to the weight loss specimens after immersion and the uncertainty of very low values of mass loss generated in very small specimens.

4. CONCLUSIONS

A study of corrosion performance from the conventional weight loss method, electrochemical noise technique and polarization curves, together with SEM and EDS analysis was obtained for the stainless steel AISI-409 exposed during 5 days to 50 mol% Na_2SO_4 –50 mol% V_2O_5 molten salt at 700°C. The results indicated that AISI-309 presented a major dissolution of the initially chromium and iron oxides layers formed during the first corrosion stage, after which a concentrated nickel oxide layer was observed under chromium oxide. Then, and during the third stage intergranular sulfidation was presented, in which it was observed the formation of nickel and iron sulphides. The optical images of AISI-309 freed from corrosion products together with the SEM mappings of the main elements of the corrosive system and EDS analysis supported these conclusions.

The electrochemical noise pattern was used to analyze the changes in corrosion activity for the system under study along the exposure time in molten salts. During the first 48 hours, the current and potential time series showed low amplitude high frequency stochastic oscillations. This noise pattern indicates the formation of a passivated film, which protected the material, whereas potential become nobler. During the second corrosion stage many high-medium transients were observed accompanied

with random oscillations, which evidences the nucleation of localized sites or the rupture and recovery of the passive film. Third stage, observed during the fifth day, showed the continuous presence of negative and positive transients of the same magnitude and the same frequency. Those changes in current, where an instantaneous and sudden increment is followed by a current decrement, showed the presence of a kind of localized events in the generalized way, such as it was observed in Figure 1.

Cumulative corrosion rate obtained from the electrochemical noise was a little higher compared to that obtained from the conventional weight loss method, which was probably due to the excessive cleaning of the samples from weight loss method.

References

1. R.A. Rapp, Y.S. Zhang, Hot Corrosion of Materials – Fundamental Aspects, Molten Salt Forum, *Trans. Technological Publications* 5–6 (1998) 25.
2. L.D. Paul, R.R. Seeley, Oil Ash Corrosion – A Review of Utility Boiler Experience, in: CORROSION/90, NACE International, Paper 911 (1990) 267.
3. Y. Harada, T. Kawamura, *Mitsubishi Technical Bulletin* 139 (1980).
4. H.J. Ratzer Scheibe, Electrochemical studies of uncoated and coated Ni-base super alloys in molten sulphate, in: 4th International Symposium on high temperature corrosion and protection of materials, France (1996) 1–8.
5. J. Uruchurtu-Chavarin, and J.M. Malo, *Trends in Corros. Research* 2, (1997) 49.
6. R. G. Kelly, "Corrosion Test and Standards Manual, Application and Interpretation" Chapter 18: Pitting. R. Baboian (ed), ASTM, Manual Series: MNL20 (1995) 166.
7. Y.F. Cheng, M. Wilmott and J.L. Luo, *Corros. Sci.* 41 (1999) 1245.
8. P.E. Doherty, D.C.A. Moore, W.M. Cox, and J.L. Dawson, An application of Advanced Electrochemical Monitoring to Corrosion of Heat Exchanger Tubing, 4th International Symposium Environmental Degradation of Materials in Power Systems, Jekyll Island, Georgia, USA, EPRI (1989) 13/65-77,
9. G.A. Whitlow, W.Y. Mok, U.M. Cox, P.J. Gallagher, S.Y. Lee and P. Elliott, On-line Materials Surveillance for Improved Reliability in Power Generation Systems, CORROSION/91, NACE-International, Paper 254 (1991).
10. G. Gao, F.H. Stott, J. L. Dawson and D. M. Farrel, *Oxid. Met.* 33 ½ (1990) 79.
11. D.M. Farrel, W. M. Cox, F. H. Stott, D. A. Eden, J. L. Dawson and G. C. Wood, *High Temp. Technol.* (1985) 15.
12. D. M. Farrell, F. H. Stott, G. Rocchini and A. Colombo, U.K. Corrosion Congress 91, Vol. 2 (Manchester European Federation of Corrosion (1991)).
13. J.R. Scully, R. Baboian (Ed.), ASTM Manual Series: MNL 20, Chapter 7 (1995) 75.
14. A. Wong-Moreno, R.I. Marchan Salgado, Molten salt corrosion of heat resisting alloys, in: CORROSION/95, NACE, Houston, TX (1995) 465.
15. E. Otero, A. Pardo, J. Hernaez and P. Hierro, *Reviews in Metal Madrid* 1 (1990) 26.
16. J.R. Wilson, Understanding and preventing fuel ash corrosion, in: CORROSION/76, NACE International (1976) 12/1–12/23.
17. A. Wong-Moreno, Y. Mujica Martinez and L. Martinez, High Temperature Corrosion enhanced by Residual Fuel Oil Ash Deposits, in: CORROSION/94, NACE International, Paper 185 (1994).
18. ASTM Standard G1: Practice for Preparing, Cleaning, and Evaluating Corrosion Test Specimens, West Conshohocken, PA: ASTM International (1994).
19. ASTM Standard G31: Practice for Laboratory Immersion Corrosion Testing of Metals, West Conshohocken, PA: ASTM International, (1995).
20. C. Cuevas Arteaga, *Corros. Sci.* 50 (2008) 650.

21. C. Cuevas Arteaga, J. Uruchurtu-Chavarín, U. Cano, J. Porcayo-Calderon, G. Izquierdo and J. González, *Corros. J.* 60 (6). (2004) 548.
22. C. Cuevas-Arteaga, J. Uruchurtu-Chavarin, J. Porcayo-Calderon, G. Izquierdo-Montalvo and J. Gonzalez, *Corros. Sci.* 46 (2004) 65.
23. H. Lewis, *British Petroleum Equipment News* 7/4-5 (1957) 17.
24. P.A. Alexander and R.A. Marsden, Corrosion of superheater materials by residual oil ash, in: International Conference on the mechanism of corrosion by fuel impurities, L.M. Wyatt and G.J. Evans (eds). Butterworths, Marchwood (1963) 542.
25. N.J.H. Small, H. Strawson and A. Lewis, Recent advances in the chemistry of fuel oil ash, in: International conference on the mechanism of corrosion by fuel impurities, L.M. Wyatt and G.J. Evans (eds), Butterworths, Marchwood (1963) 238.
26. W. Skinner, *Br. Corros. J.* 22 (3) (1987) 172.
27. R. Cottis, S. Turgoose, in B. C. Syrett (Ed), *Electrochemical Impedance and Noise*, NACE Corrosion Testing Made Easy, Houston (1999).
28. C. Breslin, A. L. Rudd, *Corros. Sci.* 42 (2000) 1023.
29. F. Mansfeld, Z. Sun, C.H. Hsu and A. Nagiub, *Corros. Sci.* 43 (2001) 341.
30. A.N. Rothwell, G.L. Edgemont and G.E.C. Bell, Data Processing for Current and Potential Logging Field Monitoring Systems, in: CORROSION/1999, NACE-International, Paper 192 (1999).
31. C. Cuevas-Arteaga, J. Porcayo-Calderón, *Mat. Sci. and Eng. A* 435-436 (2006) 439.
32. F. Mansfeld, L.T. Han, C.C. Lee, C. Chen, G. Zhang and H. Xiao, *Corros. Sci.* 39 (2) (1997) 255.
33. A.A. Alawadhi, R.A. Cottis, Proceedings of the CORROSION/1999, Paper 207, NACE International (1999) 207/1–207/24.
34. J. M. Sanchez-Amaya, R. A. Cottis and F. J. botana, *Corros. Sci.* 47 (2005) 3280.
35. F. Mansfeld, C.C. Lee and G. Zhang, *Electrochim. Acta* 43 (3/4) (1998) 435.
36. ASTM Standard G102: Practice for Calculation of Corrosion Rates and Related Information from Electrochemical Measurements (1994).
37. X.Y. Zhou, S.N. Lvov, X.J. Wei, L.G. Benning and D.D. Macdonald, *Corros. Sci.* 44 (2002) 841.